Published in final edited form as:
Mol Pharm. 2013 September 3; 10(9): 3384–3391. doi:10.1021/mp400225s.

A Novel Aliphatic ^{18}F-Labeled Probe for PET Imaging of Melanoma

Hongguang Liu[1,2,&], **Shuanglong Liu**[1,&], **Zheng Miao**[1], **Han Jiang**[1], **Zixin Deng**[3], **Xuechuan Hong**[3,*], and **Zhen Cheng**[1,*]

[1]Molecular Imaging Program at Stanford (MIPS), Bio-X Program, and Department of Radiology, Canary Center at Stanford for Cancer Early Detection, Stanford University, California, 94305-5344

[2]Institute of Molecular Medicine, College of Life and Health Science, Northeastern University, Shenyang 110004, PR China

[3]Key Laboratory of Combinatorial Biosynthesis and Drug Discovery, Wuhan University, Ministry of Education, Wuhan University School of Pharmaceutical Sciences, Wuhan 430071, People's Republic of China

Abstract

Radiofluorinated benzamide and nicotinamide analogs are promising molecular probes for the positron emission tomography (PET) imaging of melanoma. Compounds containing aromatic (benzene or pyridine) and *N*,*N*-diethylethylenediamine groups have been successfully used for development of melanin targeted PET and single-photon emission computed tomography (SPECT) imaging agents for melanoma. The objective of this study was to determine the feasibility of using aliphatic compounds as a molecular platform for the development of a new generation of PET probes for melanoma detection. An aliphatic *N*,*N*-diethylethylenediamine precursor was directly coupled to a radiofluorination synthon, *p*-nitrophenyl 2-^{18}F-fluoropropionate (^{18}F-NFP), to produce the probe *N*-(2-(diethylamino)ethyl)-2-^{18}F-fluoropropanamide (^{18}F-FPDA). The melanoma-targeting ability of ^{18}F-FPDA was further evaluated both *in vitro* and *in vivo* through cell uptake assays, biodistribution studies, and small animal PET imaging in C57BL/6 mice bearing B16F10 murine melanoma tumors. Beginning with the precursor ^{18}F-NFP, the total preparation time for ^{18}F-FPDA, including the final high-performance liquid chromatography purification step, was approximately 30 min, with a decay-corrected radiochemical yield of 79.8%. The melanin-targeting specificity of ^{18}F-FPDA was demonstrated by significantly different uptake rates in tyrosine-treated and untreated B16F10 cells *in vitro*. The tumor uptake of ^{18}F-FPDA *in vivo* reached 2.65 ± 0.48 %ID/g at 2 h post-injection (p.i.) in pigment-enriched B16F10 xenografts, whereas the tumor uptake of ^{18}F-FPDA was close to the background levels, with rates of only 0.37 ± 0.07 %ID/g at 2 h p.i. in the non-pigmented U87MG tumor mouse model. Furthermore, small animal PET imaging studies revealed that ^{18}F-FPDA specifically targeted the melanotic B16F10 tumor, yielding a tumor-to-muscle ratio of approximately 4:1 at 1 h p.i. and 7:1 at 2 h p.i. In summary, we report the development of a

*Correspondence should be sent to: Zhen Cheng, Ph.D., Molecular Imaging Program at Stanford, Canary Center at Stanford for Cancer Early Detection, Department of Radiology and Bio-X Program, 1201 Welch Road, Lucas Expansion, P095, Stanford University, Stanford, CA 94305, 650-723-7866 (Office), 650-736-7925(Fax), zcheng@stanford.edu Or Xuechuan Hong, Ph.D., Key Laboratory of Combinatorial Biosynthesis and Drug Discovery, (Wuhan University), Ministry of Education, School of Pharmaceutical Sciences, Wuhan University, Wuhan, 430071, P. R. China. xhy78@whu.edu.cn, Fax: +86-027-6875-9850; Tel: +86 027-6875-2331.
&The authors contributed equally to the work.

Supporting Information

^{18}F-FPDA PET imaging and quantification in PC3 prostate cancer models. This material is available free of charge via the Internet at http://pubs.acs.org.

novel ^{18}F-labeled aliphatic compound for melanoma imaging that can be easily synthesized in high yields using the radiosynthon ^{18}F-NFP. The PET probe ^{18}F-FPDA exhibits high B16F10 tumor-targeting efficacy and favorable *in vivo* pharmacokinetics. Our study demonstrates that aliphatic compounds can be used as a new generation molecular platform for the development of novel melanoma targeting agents. Further evaluation and optimization of ^{18}F-FPDA for melanin targeted molecular imaging are therefore warranted.

Keywords

melanoma imaging; PET; melanin; ^{18}F; Benzamide

INTRODUCTION

Melanoma is the most lethal form of skin cancer, the incidence of melanoma is increasing, particularly in light-skinned populations,[1, 2] and malignant melanoma was the second leading type of cancer for those aged 20 to 39 years old in 2009.[3, 4] While melanoma accounts for only 5% of all skin cancers, it is responsible for more than 50% of skin cancer-related deaths. Melanoma is an aggressive disease and has a strong tendency to rapidly metastasize. Furthermore, this cancer is highly resistant to conventional chemo- and radiotherapy, resulting in a median survival time of 6 months for patients with malignant metastatic melanoma.[5, 6] However, melanomas that have not metastasized beyond the primary site are highly curable by surgical excision, diagnosing malignant melanoma at the earliest stage possible is critically important to increase the survival rate through early therapeutic intervention.[3]

Molecular imaging techniques, particularly positron emission tomography (PET), are promising approaches for the early detection of melanoma.[7-12] ^{18}F-Fluoro-2-deoxy-D-glucose (^{18}F-FDG) is an analog of glucose and acts as a metabolic tracer for tumor PET. ^{18}F-FDG demonstrates high sensitivity for melanoma detection and provides high-quality PET images.[13, 14] However, the mechanism of melanoma uptake and cellular retention of ^{18}F-FDG involves increased glucose metabolism, which is also observed in many other types of tumors, surgical wounds, pneumonia, and other etiologies, including infectious or inflammatory conditions. Therefore, ^{18}F-FDG lacks the specificity required for melanoma detection and false-positive diagnoses often occur.[15-17] Indeed, some reports indicate that the overall detection rate of melanoma by ^{18}F-FDG is extremely low for occult metastatic lesions in patients with stage IB-II melanoma,[18] and ^{18}F-FDG also fails to identify metastatic lesions < 1 cm in diameter that are primarily located in common melanoma metastatic organs, such as the lungs, liver, or brain.[19] Thus, there is an urgent need to develop novel PET probes with higher specificity and sensitivity for early melanoma detection.

Melanin is an amorphous and irregular polymer that is biosynthesized *via* an essential metabolic pathway regulated by tyrosinase activity in melanocytes.[20-22] Melanin is found in melanoma cells and/or melanophages,[23, 24] and increased tyrosinase activity in malignant melanoma significantly increases the amount of melanin in the tumor tissue, making melanin a very attractive target for melanoma imaging and therapy.[25-27] More recently, melanin has also been demonstrated to be an excellent reporter for multimodality imaging including PET, magnetic resonance imaging (MRI) and photoacoustic imaging.[28] A distinct advantage of using melanin as a molecular target for imaging is that the uptake of imaging probes specifically depends on the cellular melanin content, thereby providing a selective mechanism for achieving high and specific tumor-to-background contrast.

Many small molecules containing aromatic structures bind strongly to melanin both *in vivo* and *in vitro*; these small molecules include methylene blue, chloroquine, and acridine orange.[29] The radiolabeled aromatic compound ^{123}I-*N*-(2-diethylaminoethyl 4-iodobenzamide)benzamide (^{123}I-BZA, Figure 1A) has been used for clinical studies to detect malignant melanoma and metastases using single-photon emission computed tomography (SPECT) with 81% diagnostic sensitivity, 87% accuracy, and 100% specificity.[25] Because of the attractive features of the PET modality for tumor imaging, such as high sensitivity, quantification ability, and relatively high resolution, the ^{18}F-labeled benzamide analog ^{18}F-*N*-[2-(diethylamino)ethyl]-4-fluoro-benzamide (^{18}F-FBZA, Figure 1B) has recently been developed for PET imaging of primary and metastatic melanotic melanoma.[26, 30] This novel probe displays an excellent and specific tumor-imaging quality and good tumor uptake, with 5.94 ± 1.83 %ID/g at 2 h post-injection (p.i.) in B16F10 melanoma tumor-bearing mice. Notably, the pyridine-based probes ^{18}F-N-(2-(diethylamino)-ethyl)-5-fluoropicolinamide (Figure 1C) and ^{18}F-6-fluoro-*N*-[2-(diethylamino)ethyl] pyridine-3-carboxamide (^{18}F-MEL050, Figure 1D) have been developed for melanin-targeted melanoma and metastasis imaging. These probes show many favorable features, including a high radiochemical yield, simple labeling procedure, and high tumor uptake, even at very early time points.[31-34] However, these aromatic ethylenediamine compound-based probes show relatively high uptake in some normal organs, particularly the liver. Accordingly, further studies and new strategies are necessary to develop a melanin-targeted PET probe with ideal *in vivo* performance for clinical translation.

In this study, we hypothesized that the aromatic ring structure in benzamide analogs is not necessary for a melanin-targeted PET probe and that *N*-(2-diethylaminoethyl) is the key pharmacophore that is responsible for melanin targeting. Therefore, we directly conjugated the *N*-(2-diethylaminoethyl) pharmacophore to an aliphatic to a radiofluorination synthon, *p*-nitrophenyl 2-^{18}F-fluoropropionate (^{18}F-NFP), to obtain *N*-(2-(diethylamino)ethyl)-2-^{18}F-fluoropropanamide (^{18}F-FPDA, Figure 2). The *in vivo* performance of ^{18}F-FPDA was then evaluated in mice bearing melanotic B16F10 melanomas and in an amelanotic U87MG human glioblastoma model.

MATERIALS AND METHODS

General

All the commercially obtained chemicals were of analytical grade and were used without further purification. No-carrier-added ^{18}F-fluoride was obtained from an in-house PETtrace cyclotron (GE Healthcare). Reverse-phase extraction C18 Sep-Pak cartridges were obtained from Waters and were pretreated with ethanol and water prior to use. The syringe filters and polyethersulfone membranes (pore size, 0.22 μm; diameter, 13 mm) were obtained from Nalge Nunc International. Semi-preparative reverse-phase high-performance liquid chromatography (RP-HPLC) using a Vydac protein and peptide column (218TP510; 5 μm, 250 × 10 mm) was performed using a Dionex 680 chromatography system with a UVD 170U absorbance detector and a model 105S single-channel radiation detector (Carroll & Ramsey Associates). The recorded data were processed using Chromeleon version 6.50 software. The mobile phase changed from 95% solvent A [0.1% trifluoroacetic acid (TFA) in water] and 5% B [0.1% TFA in acetonitrile (MeCN)] from 0-2 min to 35% solvent A and 65% solvent B at 32 min, with a flow rate of 5 mL/min. The analytical HPLC used the same gradient system except that the flow rate was 1 mL/min using a Vydac protein and peptide column (218TP510; 5 μm, 250 × 4.6 mm). The UV absorbance was monitored at 218 nm, and identification of the products was confirmed based on the UV spectrum acquired using a PDA detector. All instruments, including the electrospray ionization mass spectrometer

(ESI-MS), nuclear magnetic resonance (NMR) imager, and PET dose calibrator, are the same as those described in our previous publication.[12]

Small animal PET scans were performed using a microPET R4 rodent model scanner (Siemens Medical Solutions). The scanner has a computer-controlled bed and 10.8-cm transaxial and 8-cm axial fields of view (FOVs). The scanner has no septa and operates exclusively in the 3-dimensional (3D) list mode. The animals were placed near the center of the scanner FOV where the highest image resolution and sensitivity are located.

Chemistry and Radiochemistry

The synthesis of 4-nitrophenyl 2-fluoropropionate (^{19}F-NFP) was performed as follows. *bis*(4-Nitrophenyl) carbonate (15.2 mg, 50.0 μmol) and 20 μL *N*,*N*-diisopropylethylamine (DIPEA) were added to a solution of 2-fluoropropionic acid (5.0 mg, 54.3 μmol) in 200 μL *N*,*N*-dimethylformamide (DMF). After incubation at 60 °C for 3 h, the reaction mixture was cooled to room temperature and diluted with 1 mL 5% acetic acid solution. The product ^{19}F-NFP was isolated by semi-preparative HPLC. The collected fractions were combined, and the solvent was removed under reduced pressure. The product was obtained as a white powder (5.9 mg, 56%). The retention time [Rt] of the product was 24.5 min, as determined by analytical HPLC. ESI-MS, m/z = 213.3 measured for $[M]^+$ ($C_9H_8FNO_4$, calculated molecular weight of 213.1); ^{1}H NMR ($CDCl_3$, 300 MHz), δ = 8.24 (d, *J* = 9.0 Hz, 2H), 7.27 (d, *J* = 9.0 Hz, 2H), 5.21 (m, 1H), 1.70 (dd, *J* = 6.8 Hz, 23.4 Hz, 3H); ^{13}C NMR ($CDCl_3$, 75 MHz), δ = 18.9 (d, $J_{C,F}$ = 22.5 Hz), 86.0 (d, $J_{C,F}$ = 184.0 Hz), 122.9, 126.0, 146.4, 155.2, 168.5.

The synthesis of *N*-(2-(diethylamino)ethyl)-2-fluoropropanamide (^{19}F-FPDA) was performed as follows. *N*,*N*-Diethylethylenediamine (DEDA, 3.5 mg, 30 μmol) was added to a solution of ^{19}F-NFP (6.0 mg, 30 μmol) in 1 mL anhydrous DMF. After stirring at room temperature for 3 h, the product ^{19}F-FPDA was isolated by semi-preparative HPLC, with a yield of 45%. The retention time by analytical HPLC was 9.4 min. The ESI-MS was m/z 190.4 for $[M]^+$ ($C_9H_{19}FN_2O$, calculated molecular weight of 190.3). ^{1}H NMR (DMSO-d_6, 300 MHz), δ = 7.95 (br, 1H), 4.94 (dq, *J* = 6.8 Hz, 48.8 Hz, 1H), 2.97 (q, *J* = 7.1 Hz, 4H), 2.51 (t, *J* = 5.6 Hz, 2H), 2.40 (m, 2H), 1.31 (dd, *J* = 6.8 Hz, 23.2 Hz, 3H), 0.89 (t, *J* = 7.1 Hz, 6H); ^{13}C NMR (DMSO-d_6, 75 MHz), δ = 169.8 (d, $J_{C,F}$ = 19.8 Hz), 88.0 (d, $J_{C,F}$ = 179.1 Hz), 50.8, 46.6, 41.3, 18.4 (d, $J_{C,F}$ = 21.4 Hz), 13.2.

The radiofluorination synthon ^{18}F-NFP was obtained according to our previously reported protocol.[35, 36] ^{18}F-FPDA was then synthesized by direct coupling of ^{18}F-NFP with DEDA. Briefly, DEDA (5 mg) was added to a DMSO solution containing approximately 20 mCi ^{18}F-NFP. After stirring at 60 °C for 5 min, the product ^{18}F-FPDA, which displays the same retention time as ^{19}F-FPDA, was isolated by semi-preparative HPLC. The solvent from the collected fractions was removed by rotary evaporation, and the radiolabeled product was reconstituted in phosphate-buffered saline (PBS) and passed through a 0.22-μm Millipore filter into a sterile vial for *in vitro* and *in vivo* experiments.

Serum Stability of ^{18}F-FPDA

The *in vitro* stability of ^{18}F-FPDA was evaluated by incubation of 7.4 MBq (200 μCi) of the PET probe with mouse serum (1 mL) at 37 °C. At 30, 60, and 120 min, the solution was filtered through a NanoSep 10 K centrifuge (Pall Corp.) to isolate the low-molecular-weight metabolites. The filtrates were analyzed by reverse-phase HPLC using conditions identical to those used for the ^{18}F-FPDA analysis.

Cell Culture and Uptake Assay

Melanotic B16F10 melanoma cells were cultured in Dulbecco's Modified Eagle Medium high-glucose (Gibco Life Sciences) supplemented with 10% fetal bovine serum (FBS) and 50 units/ml penicillin and streptomycin. The cells were regularly maintained at 37 °C in a 5% CO_2 humidified incubator. The cellular uptake studies were performed using B16F10 cells. Briefly, approximately 1×10^6 B16F10 cells were plated in a 12-well plate with or without 2 mM L-tyrosine pre-treatment for 24 h. The cells were then incubated with Advanced Modified Eagle's Medium (MEM) containing 25 mM *N*-(2-hydroxyethyl)piperazine-*N*-(2-ethanesulfonic acid), 0.2% bovine serum albumin (BSA), 0.3 mM 1,10-phenanthroline, and 3.7 kBq (0.1 μCi) ^{18}F-FPDA for 60 min and 120 min at 4 °C. Cells not treated with tyrosine were used as a control. The cells were washed 3 times with ice-cold PBS and lysed with 0.5 N NaOH for 5 min at room temperature. The radioactivity of the cell lysate was measured using a Wallac 1480 automated γ-counter (Perkin Elmer). The percent uptake, which was calculated as the radioactivity of the cell lysate divided by the total radioactivity added for the cell incubation, was plotted as a function of time using Prism 4.0 (GraphPad). Amelanotic human U87MG glioblastoma cells were purchased from the American Type Culture Collection and cultured in Dulbecco's Modified Eagle Medium high-glucose (Gibco Life Sciences) supplemented with 10% (v/v) FBS (Invitrogen) at 37 °C in a 5% CO_2 incubator.

Animal Biodistribution Studies

All animal studies were performed according to a protocol approved by the Stanford University Institutional Animal Care and Use Committee. All mice were purchased from Charles River Laboratory. Approximately 1.0×10^6 cultured B16F10 cells were resuspended in PBS and subcutaneously implanted in the right shoulder of female C57BL/6 mice. The tumors were allowed to reach a size of 0.5 cm^3 (~ 10 day) before the mice were used for experiments. Similarly, approximately 10×10^6 cultured U87MG cells were resuspended in PBS and subcutaneously implanted in the right shoulder of either female nude mice or male nude mice, and the tumors were allowed to reach a size of 0.5 cm in diameter (3–4 weeks).

For the biodistribution studies, the tumor-bearing mice (n = 4 or 5 for each group) were administered approximately 3.7 MBq (100 μCi) ^{18}F-FPDA *via* tail vein injection and then sacrificed at 1 h p.i. and 2 h p.i. The tumor and normal tissues of interest were removed and weighed, and the radioactivity of the tissues was measured with a γ-counter. The radioactivity uptake in the tumor and normal tissues was expressed as percent of injected dose per gram of tissue (%ID/g).

Small Animal PET Imaging

For dynamic scanning, B16F10 tumor-bearing mice were injected *via* the tail vein with approximately 3.7 MBq (100 μCi) ^{18}F-FPDA; the PET scans (6 × 20 sec, 8 × 60 sec, and 10 × 150 sec, a total of 24 frames) began approximately 2.0 min after injection of the probe and continued for 35 min. For static scans, mice bearing either the B16F10 or U87MG tumor xenografts were administered approximately 3.7 MBq (100 μCi) ^{18}F-FPDA *via* tail vein injection. At 0.5 h p.i., 1 h p.i, and 2 h p.i., the mice were anesthetized with isoflurane (5% for induction and 2% for maintenance in 100% O_2) using a knock-down box. Using a laser beam attached to the scanner, the mice were placed in the prone position near the center of the field of view of the scanner, and 3-min static scans were then obtained. The images were reconstructed using a 2-dimensional ordered-subset expectation maximization (OSEM) algorithm. No background correction was performed. Regions of interest (ROIs; 5 pixels for coronal and transaxial slices) were drawn over the tumor on decay-corrected whole-body coronal images. The maximum counts per pixel per min were obtained from the ROIs and

converted to counts per milliliter per minute using a calibration constant. Assuming a tissue density of 1 g/mL, the ROIs were converted to counts per gram per min. The image ROI-derived %ID/g values were determined by dividing the counts per gram per minute by the injected dose. No attenuation correction was performed.

Statistical Analysis

The quantitative data are expressed as the mean ± SD; the means were compared using a one-way ANOVA and Student's t test. *P* values < 0.05 were considered statistically significant.

RESULTS

Chemistry and Radiochemistry

Non-radioactive ^{19}F-FPDA was synthesized in a 1-step coupling reaction between DEDA and ^{19}F-NFP (Figure 2). HPLC purification of ^{19}F-FPDA yielded approximately 45% of the desired product, with a 9.4 min retention time *via* analytical HPLC. The identity of the isolated compound was subsequently verified and confirmed by ESI-MS and NMR. For radiosynthesis, the coupling of ^{18}F-NFP and DEDA was achieved in high decay-corrected yields (79.8 ± 13.5%, n = 3). The radiochemical purity of ^{18}F-FPDA was greater than 99% according to analytical HPLC (Figure 3), and the specific activity (SA) was estimated to be approximately 20–40 TBq/mmol based on the SA of the labeling agent ^{18}F-NFP. The high and reliable yields of ^{18}F-FPDA make it possible to scale-up production or even clinically translate this PET probe for further studies.

Serum Stability of ^{18}F-FPDA

The stability of ^{18}F-FPDA in mouse serum is shown in Figure 3. The percentage of intact probe was greater than 98% during 30, 60, and 120 min of incubation at 37 °C. Defluorination was not observed for ^{18}F-FPDA, even during the 120-min incubation. Overall, ^{18}F-FPDA can be reliably produced and demonstrates excellent *in vitro* stability.

Cell Uptake of ^{18}F-FPDA

The cellular uptake of ^{18}F-FPDA at 4 °C in control non-tyrosine-treated B16F10 cells was 0.91 ± 0.08% and 0.82 ± 0.07% over a 1-h and 2-h incubation period, respectively. Pretreatment of the B16F10 cells with L-tyrosine (2.0 mM) for 24 h significantly increased melanin production compared to the control cells (Figure 4A). These tyrosine-stimulated cells displayed significant increases in ^{18}F-FPDA accumulation at 4 °C ($P < 0.05$). For example, after a 2-h incubation with tyrosine, the tyrosine-stimulated cellular uptake was 5.54 ± 0.40% of ^{18}F-FPDA, a 6-fold increase compared to the uptake of non-treated cells (Figure 4B).

Small Animal PET Imaging Studies

The *in vivo* tumor-targeting efficacy and imaging properties of ^{18}F-FPDA in B16F10 tumor-bearing mice were evaluated by 35-min dynamic microPET scans and static scans at 0.5 h p.i., 1 h p.i., and 2 h p.i. As shown in Figure 5, the probe was rapidly cleared from the renal system, as determined by a quantification analysis of the kidney uptake over time. During the first 3 min after tail vein injection of ^{18}F-FPDA, the radioactivity rapidly accumulated in the kidneys (19.7 ± 4.5 %ID/g) and was then reduced to approximately 30% (6.7 ± 0.3 %ID/g) of the highest uptake at 15 min p.i. In contrast, tumor uptake of ^{18}F-FPDA reached 3.70 ± 0.97 %ID/g at 2.5 min p.i. and then gradually increased to the highest uptake (5.36 ± 0.49 %ID/g) at approximately 16 min p.i. The tumor uptake of ^{18}F-FPDA was sustained at 4.88 ± 0.31 %ID/g (Figure 5) at the end of the 35-min dynamic scan. During all the dynamic scan

frames, the liver uptake of ^{18}F-FPDA quickly decreased from 6.15 ± 1.29 to 2.03 ± 1.35 %ID/g. Relatively low levels of ^{18}F-FPDA uptake in muscle tissue (from 1.33 ± 0.35 to 0.85 ± 0.23 %ID/g) were observed.

In the static, small-animal PET images (Figure 6A), the B16F10 tumors were clearly visible at 0.5 h, 1 h, and 2 h, with a high tumor-to-background ratio of 4, 4, and 7, respectively, whereas the amelanotic U87MG tumors were not very visible. The kidneys were also visible in all the animals, which was consistent with the renal clearance of the ^{18}F-FPDA probe that was observed in the dynamic scans. An ROI analysis of the tumor uptake of ^{18}F-FPDA showed that the B16F10 tumors had significantly higher ^{18}F-FPDA uptake than the U87MG tumors ($P < 0.05$). For example, the B16F10 and U87MG tumor uptake rates at 2 h p.i. were 3.05 ± 1.71 %ID/g and 0.28 ± 0.05 %ID/g, respectively (Figure 6B, C). The tumor-to-major-organ ratios of ^{18}F-FPDA for the B16F10 tumor model were calculated to understand the tumor-targeting efficacy and *in vivo* pharmacokinetics of ^{18}F-FPDA (Figure 6D). Although ^{18}F-FPDA had much higher tumor uptake rates at 0.5 and 1 h p.i. compared to 2 h p.i., the tumor-to-muscle ratios were significantly higher at 2 h p.i. compared to the earlier time points because of the rapid clearance of the probe from muscle. Low *in vivo* tumor uptake was also observed in low-melanin PC3 prostate cancer models (Supplemental Figure 1 and 2). Taken together, ^{18}F-FPDA can specifically target melanotic melanoma with good contrast but does not target amelanotic tumors, such as glioblastomas.

Biodistribution Studies

The results of the biodistribution study are shown in Table 1. For the B16F10 tumor-bearing mice, the tumor uptake rates for ^{18}F-FPDA were 4.39 ± 0.51 and 2.65 ± 0.48 %ID/g at 1 h p.i. and 2 h p.i., respectively; the kidney uptake rate was 4.50 ± 0.32 %ID/g at 1 h p.i. and rapidly decreased to 0.84 ± 0.16 %ID/g at 2 h p.i. ^{18}F-FPDA was also rapidly cleared from the blood, as evidenced by the low level of blood uptake (0.53 ± 0.04 %ID/g at 1 h p.i.). Notably, because of the high melanin concentration in the eyes of C57BL/6 mice, the uptake of ^{18}F-FPDA in the eyes was high at both time points, with uptake rates of 12.58 ± 1.14 and 10.16 ± 2.82 %ID/g at 1 h p.i. and 2 h p.i., respectively. Moreover, relatively low bone uptake rates of ^{18}F-FPDA were observed at 2 h p.i., and the tumor-to-bone ratios were similar at all time points examined (~ 4 at 1 h p.i. and 2 h p.i., Table 1), consistent with the high stability of ^{18}F-FPDA in mouse serum (Figure 3).

As a control, biodistribution studies were also performed with U87MG tumor-bearing mice (n = 4) at 2 h p.i., with ^{18}F-FPDA tumor uptake rates of only 0.37 ± 0.07 %ID/g, and there was no significant difference ($P > 0.05$) in comparison to the muscle uptake of ^{18}F-FPDA (0.28 ± 0.07 %ID/g) in these mice. Notably, the eye uptake of ^{18}F-FPDA was only 0.30 ± 0.06 %ID/g, 30-40-fold lower than the uptake rate of the black mouse eyes because the eyes of nude mice contain much less melanin. This result further confirmed the melanin-targeting property of ^{18}F-FPDA.

DISCUSSION

The increasing incidence of malignant melanoma has become a major health concern,[1, 2] and the lack of an effective treatment for metastatic melanoma has stimulated a great deal of research to develop new methods for the early melanoma detection. Previous efforts to develop melanin-specific probes for PET imaging have focused primarily on the synthesis of aromatic ethylenediamine derivatives, which display both melanin-specific binding and high rates of uptake by melanoma tumors in both small animal models and clinical patient-imaging studies.[25, 26, 29, 32] The important factors for in vivo performance of a melanin-binding probe include the charge and the lipophilicity of the molecule. In the present study, we removed the aromatic groups (benzenes or pyridine) from the molecular scaffold and

successfully developed an aliphatic melanin-targeting PET probe for melanoma imaging: ^{18}F-FPDA. Notably, our results suggest that the ethylene amide-amine functional group of ^{18}F-FPDA binds strongly and specifically to melanin, even though the probe does not contain an aromatic ring. This change lowered the lipophilicity of the new probe, resulting faster *in vivo* clearance and reduced background uptake. This study opens new possibilities for the design of next-generation melanin-targeting PET probes that are based on simple aliphatic ethylenediamine analogs.

Furthermore, the chemistry and radiochemistry of the synthesis of aliphatic ethylenediamine-based probes, such as $^{18/19}$F-FPDA, are straightforward and highly reproducible, and the product can easily be obtained in high yields. *In vitro* cellular uptake studies showed that treatment of B16F10 cells with L-tyrosine significantly increased the ^{18}F-FPDA uptake from 0.80 ± 0.04% to 5.54 ± 0.40% at 4 °C after a 2-h incubation, indicating that ^{18}F-FPDA uptake is associated with the melanin content of melanoma cells (Figure 4). B16F10 melanotic melanoma and human glioblastoma U87MG were used in our *in vivo* studies, with the U87MG serving as the control tumor model. PET quantification showed that the uptake of ^{18}F-FPDA in B16F10 tumor reached 5.41 ± 1.47 %ID/g at 0.5 h and remained high for up to 2 h after injection of the probe. In contrast, the uptake of ^{18}F-FPDA by the U87MG tumor was only 0.28 ± 0.05 %ID/g at 2 h p.i., which was significantly lower than the B16F10 tumors ($P < 0.01$) (Figure 6). Together with the results of the *in vitro* cellular uptake assay, the *in vivo* results further demonstrated the high targeting specificity of ^{18}F-FPDA. The dark eyes of C57BL/6 mice have higher expression of melanin in the epithelial layer of retina. In the biodistribution study, the ^{18}F-FPDA uptake in the melanin-rich eyes of the C57BL/6 mice (12.58 and 10.16 %ID/g at 1 h p.i. and 2 h p.i.) was 30–40 times higher than the eye uptake of ^{18}F-FPDA in the non-pigmented nude mice. This also demonstrates the melanin-targeting specificity of the ^{18}F-FPDA probe (Table 1). Notably, brain uptake of the ^{18}F-FPDA probe in the B16F10 mouse model reached 1.87 ± 0.21 %ID/g at 1 h p.i., suggesting that the probe can pass through the blood-brain barrier (BBB). The ^{18}F-FPDA uptake rate of the brain then decreased to 0.36 ± 0.04 %ID/g at 2 h p.i., which may be due to the lack of melanin-rich tissues in the brain. By comparison, the brain uptake rates of ^{18}F-FBZA at 1 h p.i. and 2 h p.i. were 2.45 ± 0.51 and 0.36 ± 0.05 %ID/g, respectively[10, 17]. This result is particularly important and suggests that ^{18}F-FPDA may be a promising PET probe for the imaging of melanoma brain metastases, which commonly happen in melanoma patients.

The aliphatic ^{18}F-FPDA probe showed a slightly lower tumor uptake rate when compared to such aromatic ^{18}F PET probes as ^{18}F-FBZA. For example, the tumor uptake rate of ^{18}F-FBZA in a biodistribution study was 6.47 ± 2.16 %ID/g at 1 h p.i.,[26] whereas the tumor uptake rate of ^{18}F-FPDA in our study was 4.39 ± 0.51 %ID/g at 1 h p.i. This difference in the tumor uptake rate is most likely because of the strong interaction of ^{18}F-FBZA with the aromatic rings of the melanin subunits. The tumor-to-blood ratio is quite similar for these two different probes (9.50 ± 4.53 %ID/g for ^{18}F-FBZA *vs*. 8.26 ± 0.92 %ID/g for ^{18}F-FPDA at 1 h p.i.). Furthermore, the normal organ uptake rates of ^{18}F-FPDA were much lower than ^{18}F-FBZA. For example, the liver uptake rate of ^{18}F-FBZA was reported to be 8.82 ± 2.13 %ID/g at 1 h p.i., whereas the liver uptake rate of ^{18}F-FPDA was only 1.39 ± 0.11 %ID/g (Table 1). The lung ^{18}F-FBZA uptake rate was 2.92 ± 0.40 and 0.85 ± 0.23 %ID/g at 1 h p.i. and 2 h p.i., respectively.[10, 17] In contrast, the lung ^{18}F-FPDA uptake rates at 1 h p.i. and 2 h p.i. were 1.45 ± 0.16 and 0.29 ± 0.03 %ID/g, respectively, much lower than those of ^{18}F-FBZA. Taken together, ^{18}F-FPDA demonstrated better contrast than ^{18}F-FBZA at the early time point (1 h p.i.). Furthermore, the lower liver and lung uptake rates of ^{18}F-FPDA make it more suitable for the identification of metastatic lesions in these major organs. This beneficial property of ^{18}F-FPDA may also improve the identification of melanomas that are localized to the liver and gastrointestinal tract for which anatomic imaging, such as

computerized tomography (CT), has unsatisfactory sensitivity.[37] Our future research endeavors will, therefore, focus on ethylenediamine analogs with either different lengths of aliphatic chains or different terminal amino substituents to fine-tune the lipophilicity of the probe compound and obtain a probe with even higher tumor uptake rates and lower normal organ uptake rates.

CONCLUSIONS

An ^{18}F-labeled non-aromatic dialkylamide ^{18}F-FPDA with a high specific activity and radiochemical yield was successfully synthesized. The high tumor uptake rate, excellent tumor imaging ability, and good tumor-to-normal organ ratios of the probe were demonstrated in melanotic B16F10 melanomas when compared to control U87MG tumor-bearing mice. ^{18}F-FPDA represents a promising new type of melanin-targeted PET probe and warrants further investigation. Aliphatic compounds can serve as a new generation molecular platform for the development of novel melanoma targeting agents.

Supplementary Material

Refer to Web version on PubMed Central for supplementary material.

Acknowledgments

This work was supported, in part, by Melanoma Research Alliance (ZC), NCI *In* Vivo Cellular Molecular Imaging Center (ICMIC) grant P50 CA114747, National Science and Technology Major Project of the Ministry of Science and Technology of China No. 2012ZX10004801-003-011 (XH) and Key Project of Chinese Ministry of Education No. 313040 (XH).

References

1. Rigel DS, Russak J, Friedman R. The evolution of melanoma diagnosis: 25 years beyond the ABCDs. CA Cancer J Clin. 2010; 60(5):301–16. [PubMed: 20671054]
2. Jemal A, Siegel R, Xu J, Ward E. Cancer statistics, 2010. CA Cancer J Clin. 2010; 60(5):277–300. [PubMed: 20610543]
3. Garbe C, Eigentler TK. Diagnosis and treatment of cutaneous melanoma: state of the art 2006. Melanoma Res. 2007; 17(2):117–27. [PubMed: 17496787]
4. Jennings L, Murphy GM. Predicting outcome in melanoma: where are we now? Br J Dermatol. 2009; 161(3):496–503. [PubMed: 19624540]
5. Balch CM, Soong SJ, Gershenwald JE, Thompson JF, Reintgen DS, Cascinelli N, Urist M, McMasters KM, Ross MI, Kirkwood JM, Atkins MB, Thompson JA, Coit DG, Byrd D, Desmond R, Zhang Y, Liu PY, Lyman GH, Morabito A. Prognostic factors analysis of 17,600 melanoma patients: validation of the American Joint Committee on Cancer melanoma staging system. J Clin Oncol. 2001; 19(16):3622–34. [PubMed: 11504744]
6. Miller AJ, Mihm MC Jr. Melanoma. N Engl J Med. 2006; 355(1):51–65. [PubMed: 16822996]
7. Ren G, Pan Y, Cheng Z. Molecular probes for malignant melanoma imaging. Curr Pharm Biotech. 2010; 11(6):590–602.
8. Gambhir SS. Molecular imaging of cancer with positron emission tomography. Nature reviews. Cancer. 2002; 2(9):683–93.
9. Ren G, Liu S, Liu H, Miao Z, Cheng Z. Radiofluorinated rhenium cyclized alpha-MSH analogues for PET imaging of melanocortin receptor 1. Bioconjug Chem. 2010; 21(12):2355–60. [PubMed: 21073170]
10. Ren G, Liu Z, Miao Z, Liu H, Subbarayan M, Chin FT, Zhang L, Gambhir SS, Cheng Z. PET of malignant melanoma using 18F-labeled metallopeptides. J Nucl Med. 2009; 50(11):1865–72. [PubMed: 19837749]

11. Cheng Z, Xiong Z, Subbarayan M, Chen X, Gambhir SS. 64Cu-labeled alpha-melanocyte-stimulating hormone analog for microPET imaging of melanocortin 1 receptor expression. Bioconjug Chem. 2007; 18(3):765–72. [PubMed: 17348700]
12. Cheng Z, Zhang L, Graves E, Xiong Z, Dandekar M, Chen X, Gambhir SS. Small-animal PET of melanocortin 1 receptor expression using a 18F-labeled alpha-melanocyte-stimulating hormone analog. J Nucl Med. 2007; 48(6):987–94. [PubMed: 17504880]
13. Rigo P, Paulus P, Kaschten BJ, Hustinx R, Bury T, Jerusalem G, Benoit T, Foidart-Willems J. Oncological applications of positron emission tomography with fluorine-18 fluorodeoxyglucose. European Journal of Nuclear Medicine. 1996; 23(12):1641–74. [PubMed: 8929320]
14. Steinert HC, Huch Boni RA, Buck A, Boni R, Berthold T, Marincek B, Burg G, von Schulthess GK. Malignant melanoma: staging with whole-body positron emission tomography and 2-[F-18]-fluoro-2-deoxy-D-glucose. Radiology. 1995; 195(3):705–9. [PubMed: 7753998]
15. Eigtved A, Andersson AP, Dahlstrom K, Rabol A, Jensen M, Holm S, Sorensen SS, Drzewiecki KT, Hojgaard L, Friberg L. Use of fluorine-18 fluorodeoxyglucose positron emission tomography in the detection of silent metastases from malignant melanoma. European Journal of Nuclear Medicine. 2000; 27(1):70–5. [PubMed: 10654150]
16. Holder WD Jr, White RL Jr, Zuger JH, Easton EJ Jr, Greene FL. Effectiveness of positron emission tomography for the detection of melanoma metastases. Ann Surg. 1998; 227(5):764–9. discussion 769-71. [PubMed: 9605668]
17. Tyler DS, Onaitis M, Kherani A, Hata A, Nicholson E, Keogan M, Fisher S, Coleman E, Seigler HF. Positron emission tomography scanning in malignant melanoma. Cancer. 2000; 89(5):1019–25. [PubMed: 10964332]
18. Choi EA, Gershenwald JE. Imaging studies in patients with melanoma. Surg Oncol Clin N Am. 2007; 16(2):403–30. [PubMed: 17560520]
19. Belhocine TZ, Scott AM, Even-Sapir E, Urbain JL, Essner R. Role of nuclear medicine in the management of cutaneous malignant melanoma. J Nucl Med. 2006; 47(6):957–67. [PubMed: 16741305]
20. Jimbow K, Miyake Y, Homma K, Yasuda K, Izumi Y, Tsutsumi A, Ito S. Characterization of melanogenesis and morphogenesis of melanosomes by physicochemical properties of melanin and melanosomes in malignant melanoma. Cancer Res. 1984; 44(3):1128–34. [PubMed: 6318981]
21. Prota G. Melanins, melanogenesis and melanocytes: looking at their functional significance from the chemist's viewpoint. Pigment Cell Res / sponsored by the European Society for Pigment Cell Research and the International Pigment Cell Society. 2000; 13(4):283–93.
22. Iozumi K, Hoganson GE, Pennella R, Everett MA, Fuller BB. Role of tyrosinase as the determinant of pigmentation in cultured human melanocytes. J Invest Dermatol. 1993; 100(6): 806–11. [PubMed: 8496620]
23. Lazova R, Klump V, Pawelek J. Autophagy in cutaneous malignant melanoma. J Cutan Pathol. 2010; 37(2):256–68. [PubMed: 19615007]
24. Revskaya E, Jongco AM, Sellers RS, Howell RC, Koba W, Guimaraes AJ, Nosanchuk JD, Casadevall A, Dadachova E. Radioimmunotherapy of experimental human metastatic melanoma with melanin-binding antibodies and in combination with dacarbazine. Clin Cancer Res. 2009; 15(7):2373–9. [PubMed: 19293257]
25. Michelot JM, Moreau MF, Veyre AJ, Bonafous JF, Bacin FJ, Madelmont JC, Bussiere F, Souteyrand PA, Mauclaire LP, Chossat FM, et al. Phase II scintigraphic clinical trial of malignant melanoma and metastases with iodine-123-N-(2-diethylaminoethyl 4-iodobenzamide). J Nucl Med. 1993; 34(8):1260–6. [PubMed: 8326382]
26. Ren G, Miao Z, Liu H, Jiang L, Limpa-Amara N, Mahmood A, Gambhir SS, Cheng Z. Melanin-targeted preclinical PET imaging of melanoma metastasis. J Nucl Med. 2009; 50(10):1692–9. [PubMed: 19759116]
27. Cheng Z, Mahmood A, Li H, Davison A, Jones AG. [99mTcOAADT]-(CH2)2-NEt2: a potential small-molecule single-photon emission computed tomography probe for imaging metastatic melanoma. Cancer Res. 2005; 65(12):4979–86. [PubMed: 15958536]

28. Qin CX, Cheng K, Chen K, Hu X, Liu Y, Lan XL, Zhang YX, Liu HG, Xu YD, Bu LH, Su XH, Zhu XH, Meng SX, Cheng Z. Tyrosinase as a multifunctional reporter gene for Photoacoustic/MRI/PET triple modality molecular imaging. Sci Rep-Uk. 2013; 3

29. Ings RM. The melanin binding of drugs and its implications. Drug Metab Rev. 1984; 15(5-6): 1183–212. [PubMed: 6396056]

30. Garg S, Kothari K, Thopate SR, Doke AK, Garg PK. Design, synthesis, and preliminary in vitro and in vivo evaluation of N-(2-diethylaminoethyl)-4-[18F]fluorobenzamide ([18F]-DAFBA): a novel potential PET probe to image melanoma tumors. Bioconjug Chem. 2009; 20(3):583–90. [PubMed: 19222206]

31. Denoyer D, Potdevin T, Roselt P, Neels OC, Kirby L, Greguric I, Katsifis A, Dorow DS, Hicks RJ. Improved detection of regional melanoma metastasis using 18F-6-fluoro-N-[2-(diethylamino)ethyl] pyridine-3-carboxamide, a melanin-specific PET probe, by perilesional administration. J Nucl Med. 2011; 52(1):115–22. [PubMed: 21149487]

32. Denoyer D, Greguric I, Roselt P, Neels OC, Aide N, Taylor SR, Katsifis A, Dorow DS, Hicks RJ. High-contrast PET of melanoma using (18)F-MEL050, a selective probe for melanin with predominantly renal clearance. J Nucl Med. 2010; 51(3):441–7. [PubMed: 20150254]

33. Greguric I, Taylor SR, Denoyer D, Ballantyne P, Berghofer P, Roselt P, Pham TQ, Mattner F, Bourdier T, Neels OC, Dorow DS, Loc'h C, Hicks RJ, Katsifis A. Discovery of [18F]N-(2-(diethylamino)ethyl)-6-fluoronicotinamide: a melanoma positron emission tomography imaging radiotracer with high tumor to body contrast ratio and rapid renal clearance. J Med Chem. 2009; 52(17):5299–302. [PubMed: 19691348]

34. Liu H, Liu S, Miao Z, Deng Z, Shen B, Hong X, Cheng Z. Development of 18F-labeled picolinamide probes for PET imaging of malignant melanoma. J Med Chem. 2013; 56(3):895–901. [PubMed: 23301672]

35. Liu S, Liu Z, Chen K, Yan Y, Watzlowik P, Wester HJ, Chin FT, Chen X. 18F-labeled galacto and PEGylated RGD dimers for PET imaging of alphavbeta3 integrin expression. Mol Imaging Biol. 2010; 12(5):530–8. [PubMed: 19949981]

36. Liu S, Liu H, Ren G, Kimura RH, Cochran JR, Cheng Z. PET Imaging of Integrin Positive Tumors Using F Labeled Knottin Peptides. Theranostics. 2011; 1:403–12. [PubMed: 22211146]

37. Lens M, Bataille V, Krivokapic Z. Melanoma of the small intestine. Lancet Oncol. 2009; 10(5): 516–21. [PubMed: 19410196]

Abbreviations

PET	positron emission tomography
HPLC	high-performance liquid chromatography
p.i.	post injection

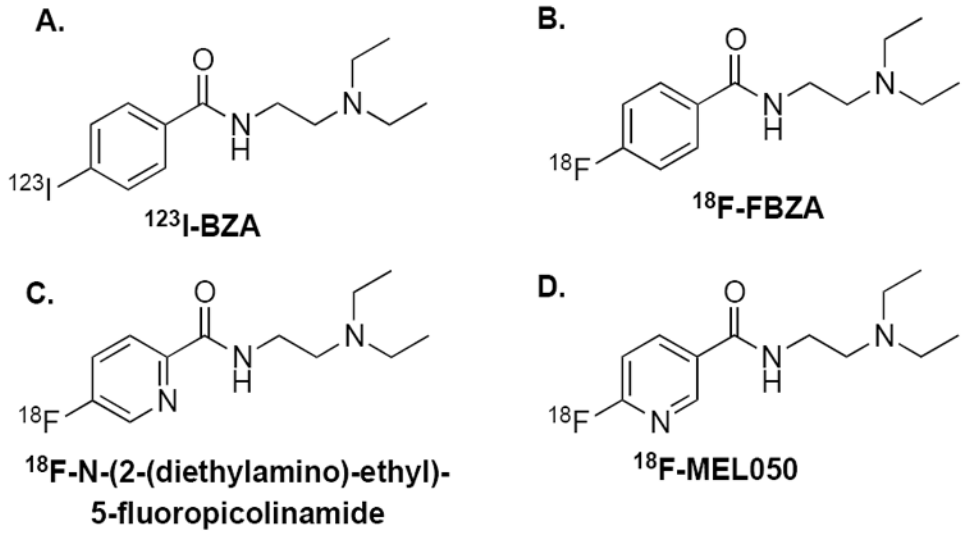

Figure 1.
Structures of the melanin-targeting melanoma probes.

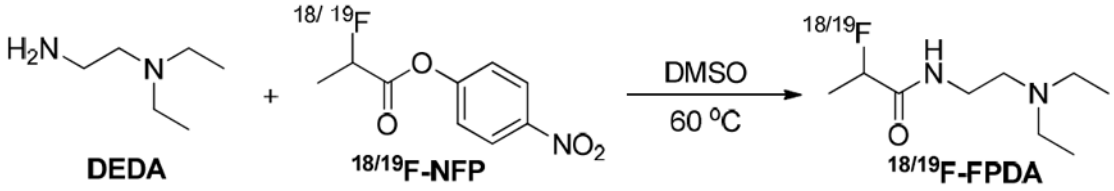

Figure 2.
The structure and chemical synthesis of $^{18/19}$F-FPDA.

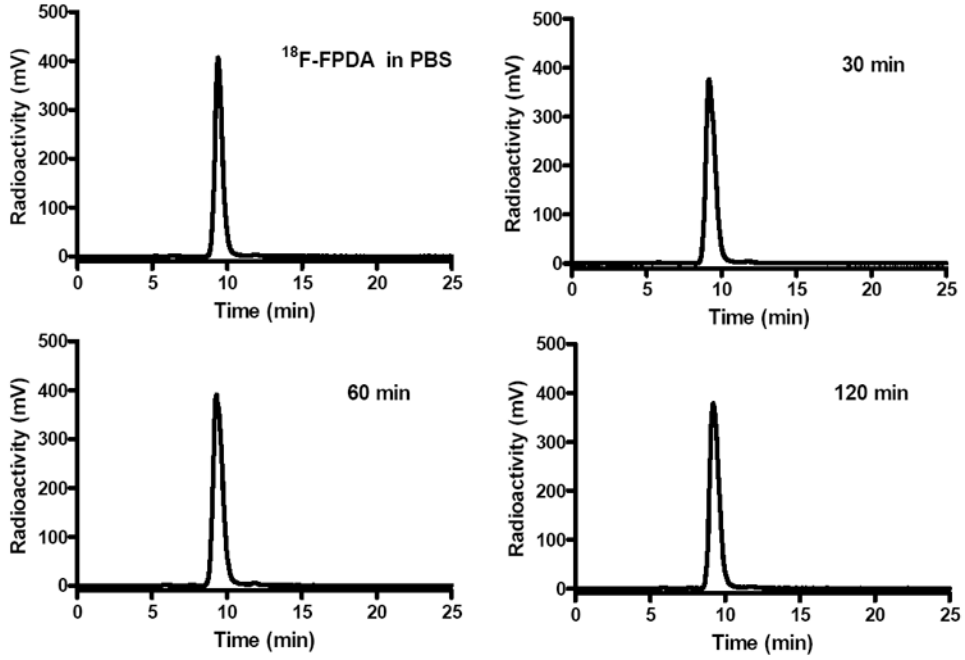

Figure 3.
^{18}F-FPDA stability in mouse serum after incubation at 37 °C for 30 min, 60 min, and 120 min.

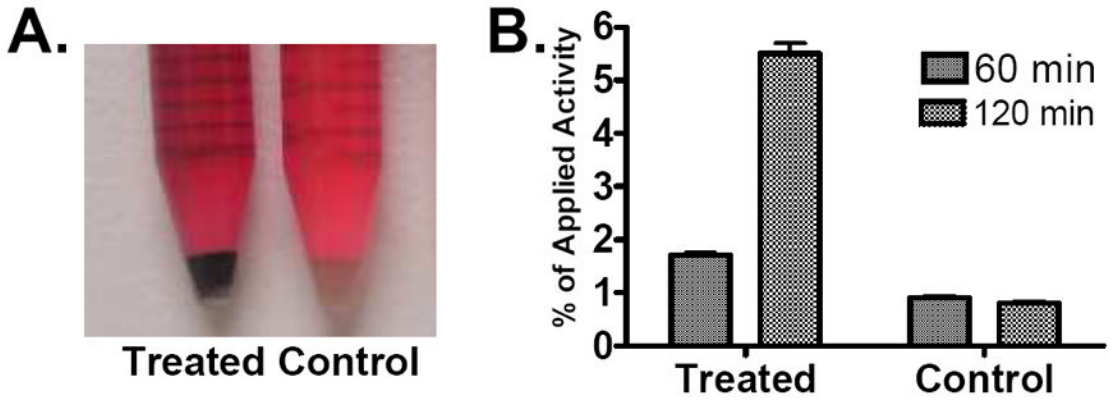

Figure 4.

(A) A digital photo of B16F10 cell pellets with (left) or without (right) L-tyrosine treatment for 24 h. (B) *In vitro* cellular uptake of ^{18}F-FPDA at 60 and 120 min at 4 °C. The data are expressed as the mean ± SD, with each data point representing studies performed in quadruplicate.

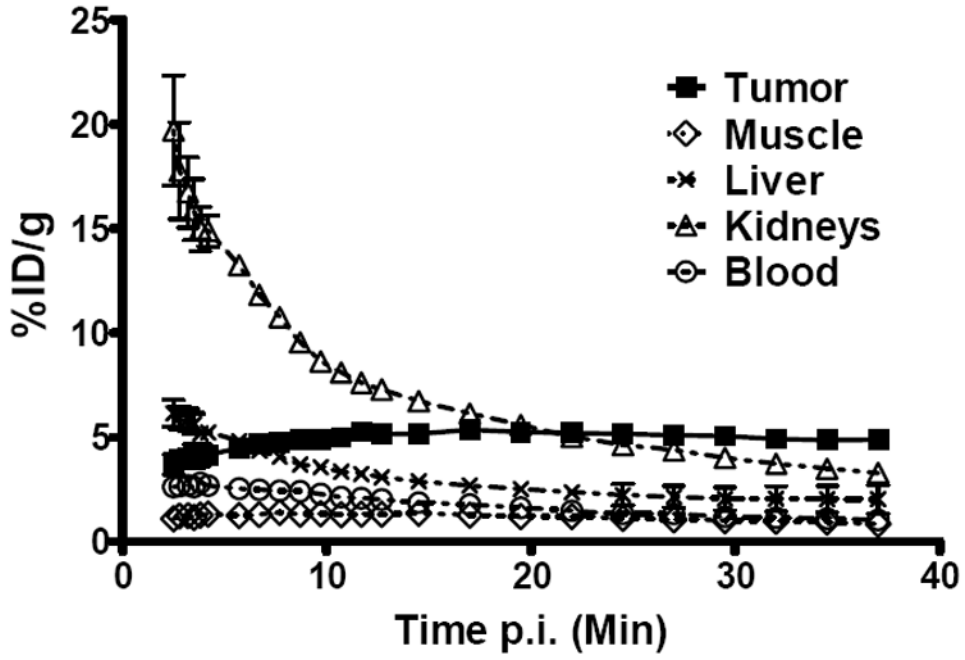

Figure 5.

Time–activity curves of tumors and major organs from male C57BL/6 mice bearing B16F10 tumors. The data are from 35-min dynamic scans following intravenous injection of ^{18}F-FPDA (~100 μCi/mouse, n = 4).

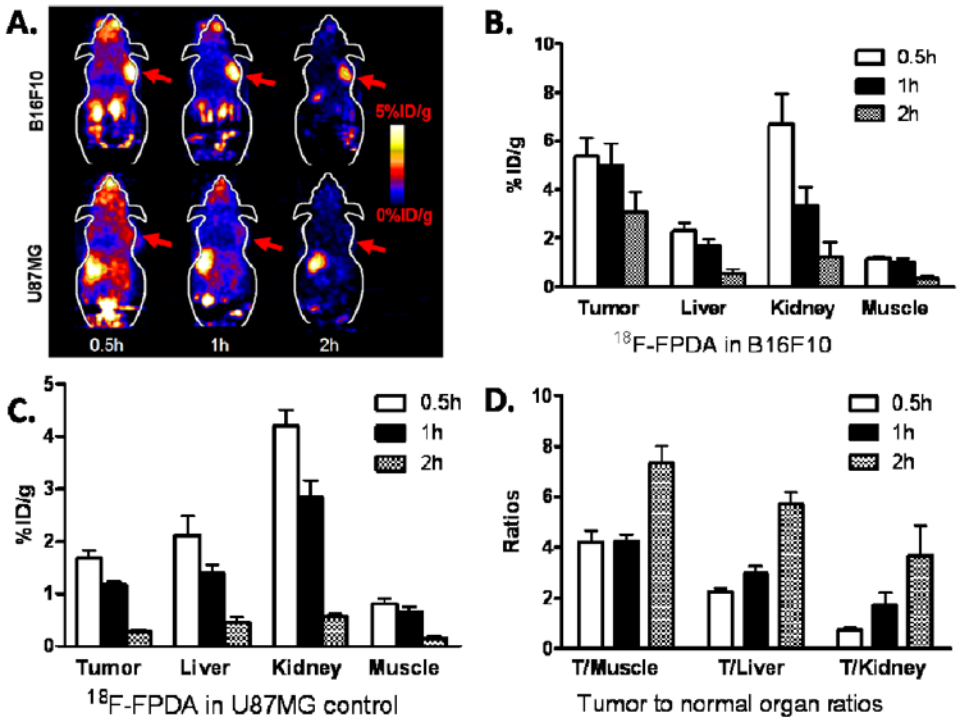

Figure 6.

Small animal PET imaging and quantification. (A) Decay-corrected whole-body coronal PET images of mice bearing B16F10 and U87MG tumors from static scans at 0.5 h, 1 h, and 2 h after the injection of ^{18}F-FPDA. The tumors are indicated with red arrows. (B) Decay-corrected PET quantification of male C57BL/6 mice bearing B16F10 tumors from static scans at 0.5 h, 1 h, and 2 h after the injection of ^{18}F-FPDA. (C) Decay-corrected PET quantification of athymic female nude mice bearing U87MG tumors from static scans at 0.5 h, 1 h, and 2 h after the injection of ^{18}F-FPDA. (D) The tumor-to-normal organ ratios of B16F10 tumor-bearing mice at 0.5 h, 1 h, and 2 h after the injection of ^{18}F-FPDA.

Table 1

^{18}F-FPDA Biodistribution Results in B16F10 and U87MG Tumor-Bearing Mice. The data are expressed as %ID/g ± SD.

	B16F10		U87 MG
Organ	**1 h n = 5**	**2 h n = 5**	**2 h n = 4**
Tumor	4.39 ± 0.51	2.65 ± 0.48	0.37 ± 0.07
Blood	0.53 ± 0.04	0.12 ± 0.01	0.16 ± 0.04
Heart	0.84 ± 0.07	0.18 ± 0.02	0.20 ±0.04
Lungs	1.45 ± 0.16	0.29 ± 0.03	0.30 ± 0.06
Liver	1.39 ± 0.11	0.30 ± 0.04	0.28 ± 0.06
Spleen	1.68 ± 0.19	0.39 ±0.07	0.43 ±0.08
Pancreas	1.56 ± 0.33	0.34 ± 0.03	0.28 ± 0.10
Stomach	4.45 ± 0.55	1.12 ± 0.49	1.07 ± 0.47
Brain	1.87 ± 0.21	0.36 ± 0.04	0.38 ± 0.07
Intestine	1.89 ± 0.95	0.96 ± 1.13	0.33 ± 0.14
Kidneys	4.50 ± 0.32	0.84 ± 0.16	0.68 ± 0.24
Skin	1.09 ± 0.43	0.23 ± 0.07	0.28 ± 0.05
Muscle	1.25 ± 0.14	0.39 ± 0.18	0.28 ± 0.07
Bone	1.57 ± 1.23	0.39 ± 0.15	0.28 ± 0.10
Eyes	12.58 ± 1.14	10.16 ± 2.82	0.30 ± 0.06
Uptake ratio			
T/Blood	8.26 ± 0.92	14.11 ± 2.87	2.34 ± 0.13
T/Liver	3.18 ± 0.44	5.81 ± 1.27	1.31 ± 0.06
T/Kidneys	0.97 ± 0.06	2.15 ± 0.50	0.56 ± 0.08
T/Bone	3.63 ± 1.37	4.70 ± 1.06	1.41 ± 0.35